

Behavior of Rubbercrete Long-Columns Subjected to Axial Loads with Minimum Eccentricity: A Numerical Study

Mohamed Salem* and Mohamed S. Issa

*Reinforced Concrete Institute, Housing and Building National Research Center, Cairo, Egypt.
(Corresponding author: mm.aladawy@gmail.com)

ABSTRACT

The study aims to evaluate the structural behavior of reinforced rubbercrete long-columns under axial load of small eccentricity. ABAQUS finite element software was employed in this study to investigate the effects of concrete compressive strengths ($f_c' = 24, 28, 60$ MPa), crumb rubber content (0.5%, 10%, 20% fine aggregate replacement) and the slenderness ratio ($\lambda = 8.0, 15, 20, 25$) on columns load capacity and lateral deflection. The results of this study show that concrete with tire rubber has lower column capacity and higher lateral deflection than the control concrete. Also, the results show that the ultimate capacity decreases and deflection increases when the slenderness ratio increases. The strengths of the original control columns have no such trend for the lateral deflection for columns with similar rubber content. It is found that the lateral deflection equations based on the Eurocode2, and ECP203-2020 code have to be more conservative in the case of the column with crumb. The studies of the current research can contribute to improvement of the recommended design and construction standards related to rubbercrete columns and their structural performance in construction. This work has possible sustainable advantages due to its application of recycled material (rubber from tires) in concrete mix.

Keywords: Rubbercrete, Crumb rubber, Concrete columns, Eccentric, Slenderness, Finite Element Modeling.

1. Introduction

Concrete production in the construction industry consumes a significant amount of natural aggregates. Additionally, a large number of rubber tires are discarded annually, creating a serious environmental challenge. A green solution is recycling these tires by using their rubber as replacement of fine natural aggregates in concrete. Rubber crumbs from recycled tires can be used to reduce waste and save natural resources. This method normally includes grinding used tires into fine particles, which can be used into construction materials, such as rubbercrete.

The mechanical properties of concrete with crumb replacement are of interest. Concrete with rubber is characterized by lesser elastic modulus which results in being a better energy absorber. This concrete has good vibration damping characteristics which make them suitable for pavements. The compressive and tensile properties of crumb concrete are lower than those of conventional concrete. There must be a limit on the added amount of rubber particles from tires to control the reduction on strengths of rubberized concrete. The material properties of rubberized concrete are studied by many researchers, for example references [1-19]. Some researchers added fibers to increase the mechanical characteristics of concrete. The properties are improved due to bridging the cracks as shown in references [20-22]. Other researchers

improved the properties of crumb concrete using rubber which is pre-treated by heat and using water which has been passed on a magnetic field as shown by reference [23].

Research on the application of rubberized concrete to structural members is limited. Youssf et al. [24] performed tests on rubber concrete columns subjected to seismic loads. They tested three columns under axial and cyclic loads. The use of crumb concrete resulted in higher damping and energy dissipation. The lateral load and displacement were little less than those of concrete columns with no crumb. Son et al. [25] studied experimentally crumb concrete columns under axial load. They tested twelve short columns of concrete strengths equal to 24 and 28 MPa. They concluded that concrete with rubber shows good ductility.

The current research targets to enhance, using the calibrated FE modeling, the shortage in knowledge on structural behavior of short and long columns made of normal and high strength reinforced concrete with tire rubber replacements of up to 20% and under axial load of minimum eccentricity. The research here is novel in addressing long columns and high strength concrete. The finite element is used to expand the limited available experimental work considering wide range of concrete strengths, rubber contents, and slenderness ratios. The project starts by modeling experimental work from literature. Then, parametric study is performed using

FE analysis. The behavior of such columns is studied, and the codes' equations are evaluated.

Son et al. [25] carried out experiments on twelve concrete columns with design strengths of 24 MPa and 28 MPa. The columns contained waste tire particles with sizes of 0.6 mm by 1.0 mm and were mixed at 0.5% of 1% by weight of total aggregate which is equivalent to volume fractions of 2.7% – 5.4%. Each column had a cross-sectional area of 200 mm x 300 mm and a length of 1600 mm; in it, there were six longitudinal bars with a diameter of 13 mm and stirrups with a diameter of 10 mm placed at a distance of 154 mm from one another, with a characteristic yield strength of 400 MPa. The concrete cover to the stirrups was maintained at 30 mm as depicted in Figure 1.

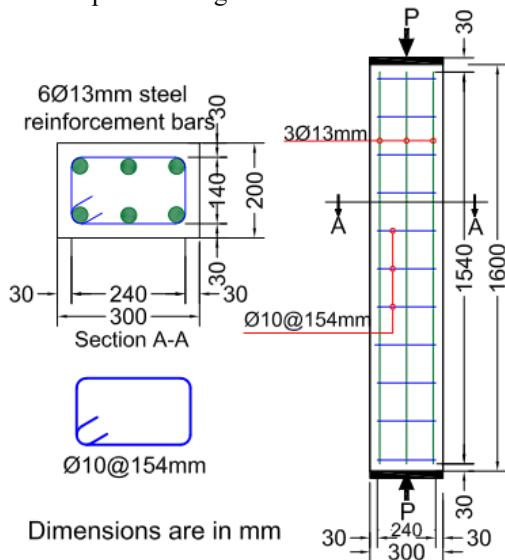


Figure 1- Experimental specimens' details tested by Son et al. [25].

2. FE Modeling of the Columns

The behavior of the crumb concrete column was studied through a finite element (FE) analysis performed with the ABAQUS program 2021 [26]. The simulation model was specifically created to verify and validate the experimental results obtained by Son et al. [25]. Due to the limited experimental data, the finite element program is calibrated against the research of Son et al (2011) [25] only. However, the utilized FEM program (ABAQUS) is widely used for modeling of reinforced concrete. The same modeling technique is also used for the columns of parametric study.

2.1. FE Modeling of Materials

Three-dimensional finite element (3D FE) models were implemented using ABAQUS software, version 2021 [26]. The materials employed in the modeling process are detailed as follows.

2.1.1. Concrete / Rubbercrete

In the ABAQUS simulation, the damage plasticity model was employed to replicate concrete behavior. This model considers two primary failure mechanisms: compression crushing and tensile cracking [26]. For the uniaxial compression behavior of normal /high-strength and rubbercrete concrete, relationship between stress and strain is considered to be linear up to 40% of the peak strength (f'_c). This assumption is widely accepted. To evaluate the compressive stress-strain curve for both normal-strength and high-strength concrete materials, the modified formula proposed by Wee et al. in 1996 was utilized [27].

From the point of 40% of f'_c to the maximum compressive strength (f'_c), the curve has the following equation for this ascending part:

$$f_c = f'_c \left(\frac{\beta(\varepsilon/\varepsilon_0)}{\beta - 1 + (\varepsilon/\varepsilon_0)^\beta} \right) \quad (1)$$

where:

$$\beta = \frac{1}{1 - \frac{f'_c}{\varepsilon_0 E_c}} \quad (2)$$

$$E_c = 4700\sqrt{f'_c} \quad (3)$$

$$\varepsilon_0 = \frac{1.71 f'_c}{E_c} \quad (4)$$

For the descending branch of the stress-strain curve beyond f'_c :

$$f_c = f'_c \left(\frac{k_1 \beta (\varepsilon/\varepsilon_0)}{k_1 \beta - 1 + (\varepsilon/\varepsilon_0)^{k_2 \beta}} \right) \quad (5)$$

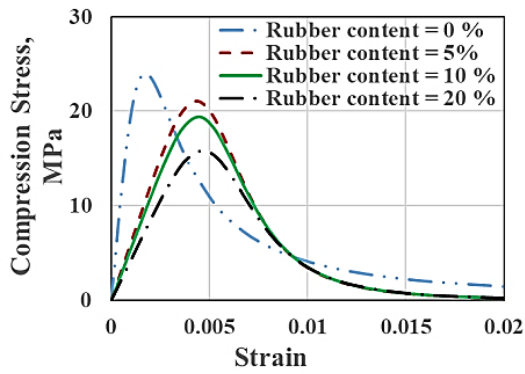
where:

$$k_1 = \left(\frac{50}{f'_c} \right)^3 \quad (6)$$

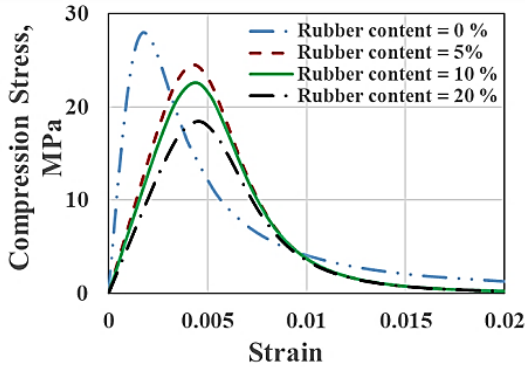
$$k_2 = \left(\frac{50}{f'_c} \right)^{1.3} \quad (7)$$

The modified stress-strain relations proposed by Aslani et al. in 2018 [28] were used to estimate the compressive stress-strain curves for rubbercrete materials. Figure 2 presents the stress- inelastic strain curves for the concrete and rubbercrete materials in the current analysis at different rubber content ratios.

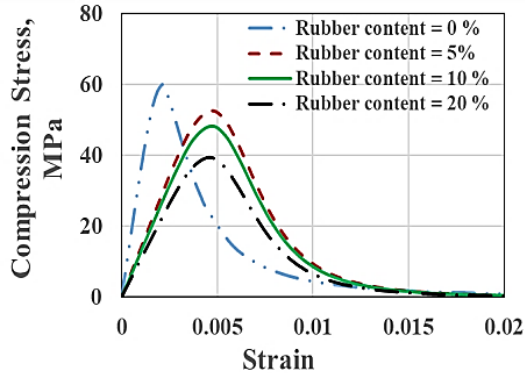
To define the concrete/rubbercrete constitutive relationship in tension, the bilinear model proposed by Coronado and Lopez is employed [29]. This bilinear model was compared to other models in their paper and found to give the best results. Figure 3 illustrates the tensile stress-cracking displacement curves for the concrete/rubbercrete materials in the simulation.



(a) $f_c' = 24 \text{ MPa}$

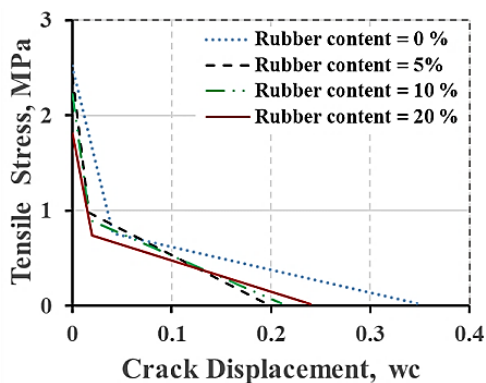


(b) $f_c' = 28 \text{ MPa}$

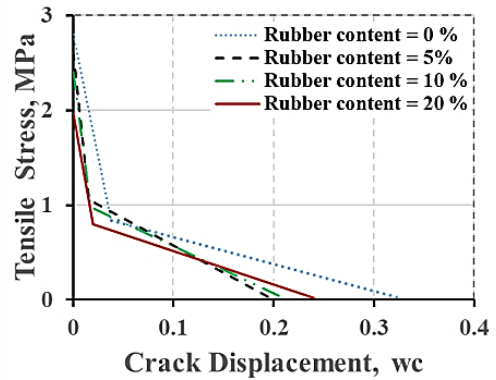


(c) $f_c' = 60 \text{ MPa}$

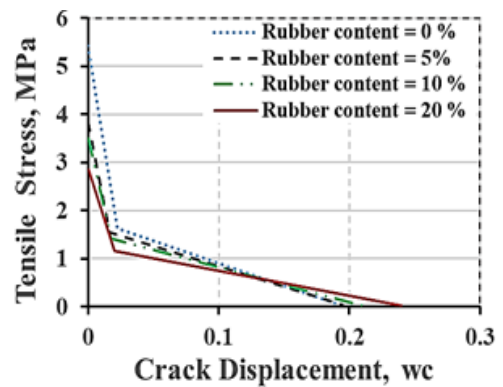
Figure 2- Concrete/Rubbercrete compressive stress-strain curves.



(a) $f_c' = 24 \text{ MPa}$



(b) $f_c' = 28 \text{ MPa}$



(c) $f_c' = 60 \text{ MPa}$

Figure 3- Concrete/rubbercrete tensile stress-cracking displacement curves.

2.1.2. Steel Reinforcement

The stress-strain relationship for the steel reinforcement bars is considered to be elastic-perfect plastic, as illustrated in Figure 4. This relationship is applied to both stirrups and longitudinal bars. A full bond is assumed between concrete and reinforcing bars. It is not expected that the limited used ratios of rubber content would affect this bond.

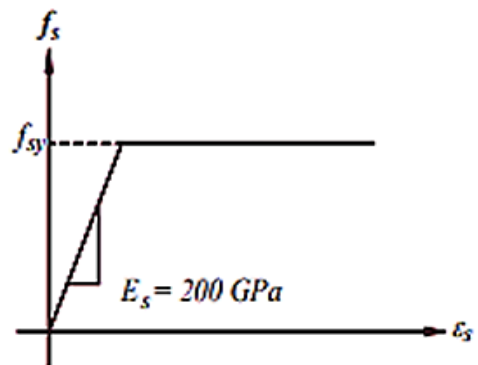


Figure 4- Stress-strain relationship for steel reinforcement

2.2. 3D Model of Column

Reinforced concrete/rubbercrete columns were simulated using a 3D ABAQUS/Standard model. Figure 5 displays the details of finite element model of column specimens in terms of geometry, shear and longitudinal reinforcement, meshes, the interactions, and boundary conditions.

For the analysis, a displacement control approach was utilized, where the top of the loading column was subjected to a displacement load in the opposite direction of the Y-axis.

The concrete in the model was represented using a reduced integration C3D8R element type which does not suffer from the locking phenomena observed in the C3D8 element. In conclusion, while using C3D8R or C3D10M elements are taken into consideration as suitable for simulating rubbercrete in Abaqus. The steel reinforcement was modeled using a 2-node linear 3-D truss element (T3D2). Additionally, a full bond between all reinforcement and concrete was assumed in the simulation.

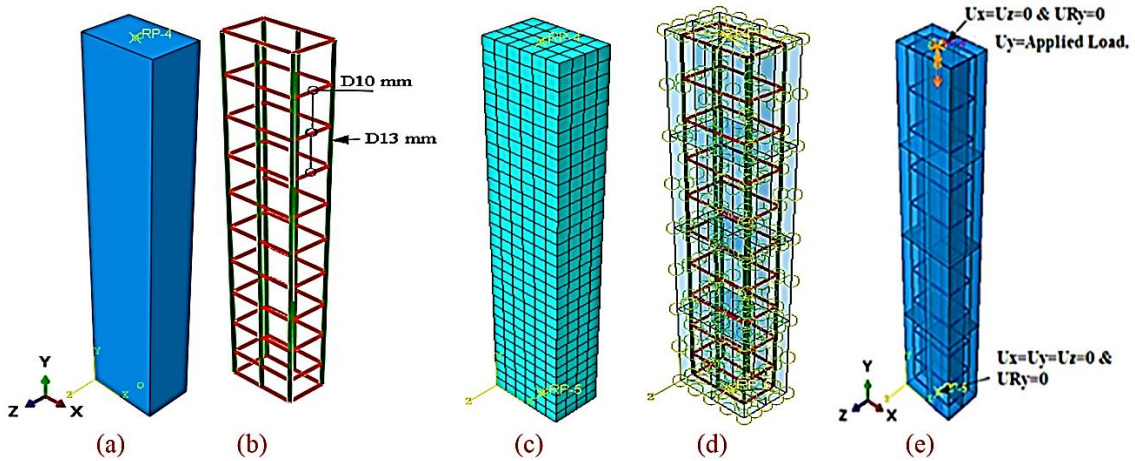


Figure 5- Details of the FE model: (a) geometry, (b) steel reinforcement, (c) meshes, (d) interactions, (e) boundary conditions and applied load

2.3. Model Validation

The proposed model was validated based on the experimental results provided by Son et al. 2011 [25] for failure-mode and ultimate capacity. FE model column failure mode shown in Figure 6 were in good agreement with column failure mode obtained from experimental test. Furthermore, the numerical results for the ultimate capacity of the beam were

observed to be in good comparison with the experimental test results as demonstrated in Figure 7. Therefore, the FE model is suitable for predicting the response of concrete/rubbercrete column. Comparison numerical as well as experimental results are presented in both Figure 6 and Figure 7.

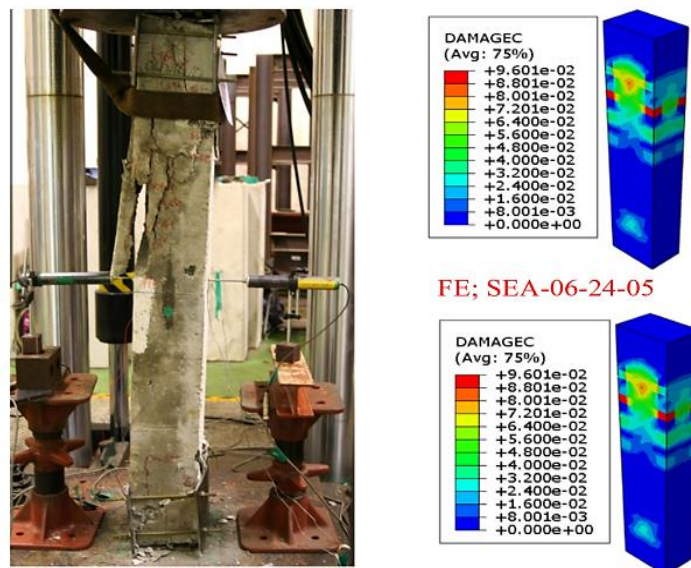


Figure 6- Failure modes of experimental and FE model column specimens

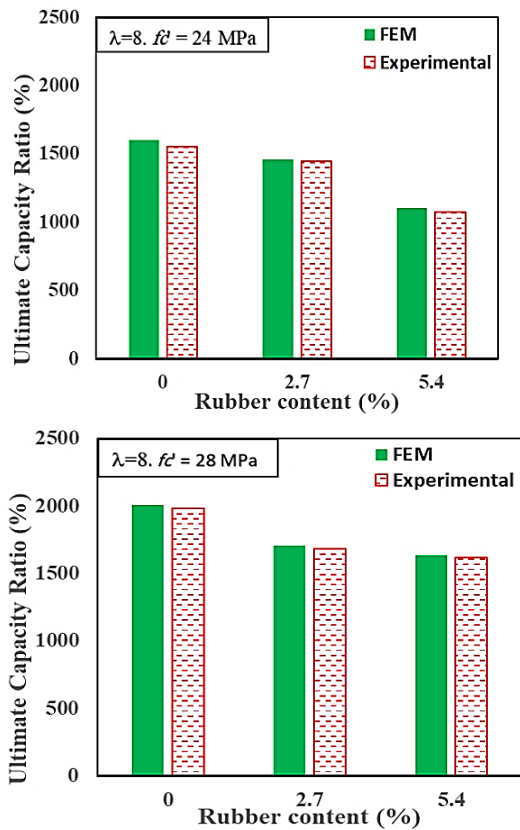


Figure 7- Comparison of ultimate capacities obtained from the FE simulations and experimental tests

2.4. Mesh Size Sensitivity

To determine the suitable finite element mesh size which presents an optimization between the required accuracy and the computational time, three computer runs are made for specimen SEA-10-28-05 of Son et al. [25] with the following mesh sizes: 50 mm, 35 mm, and 20 mm. The obtained finite element solutions for the different mesh sizes and the experimental maximum load are given in Table 1. Based on the presented results, it is decided to carry the parametric study runs using a mesh of size 20 mm which presents a good trade between the required accuracy and computational time. Good conversion of the finite element solutions is noticed in the made simulation.

Table 1- Experimental and FE solutions for specimen SEA-10-28-05 (Son et al., 2011) [25].

	Experimental	FE		
		Mesh 50 mm	Mesh 35 mm	Mesh 20 mm
Max. Load (kN)	1695	1750.6	1738.2	1711.8

3. Parametric Study

The calibrated finite element model, made using ABAQUS software, was utilized to examine the influence of various parameters on the structural behavior of short and long columns made from concrete containing tire rubber. The study considered three factors:

1. Concrete Compressive Strength: The compressive strength of the concrete cylinder, without rubber, was varied at 24, 28, and 60 MPa, representing normal and high-strength concrete.
2. Slenderness Ratio: The slenderness ratio was adjusted by changing the column length to 1600 mm, 3000 mm, 4000 mm, and 5000 mm, while maintaining a constant cross-section of 200 mm x 300 mm. This results in slenderness ratios of 8, 15, 20, and 25, respectively.
3. Rubber Content Ratio: Rubber content ratio, expressed as a percentage of the total aggregate volume, varied at 0%, 5%, 10%, and 20%.

The longitudinal reinforcements and stirrups used were 6Φ13 mm and Φ10 mm at 154 mm spacing, respectively, with a yield strength of 400 MPa. For clarity, the naming convention for the finite element runs is exemplified by Specimen S-8-24-5, which denotes a column with a slenderness ratio of 8, a concrete compressive strength of 24 MPa (for the specimen without rubber), and a rubber content ratio of 5%.

The applied load eccentricity was determined according to ECP203-2020 [30] specifications for minimum eccentricity, which is the greater of 0.05 times the side length or 20 mm. In this study, the load was applied with a minimum eccentricity of 20 mm from the centerline, along the column's smaller width, as depicted in Figure 8.

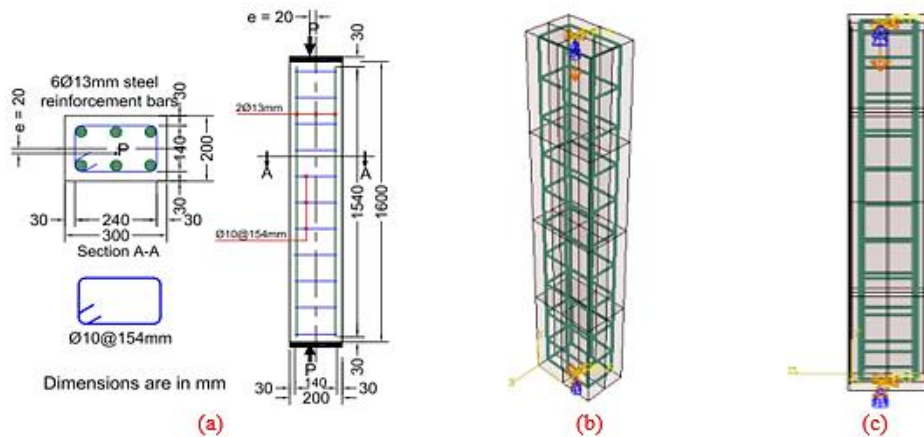


Figure 8- Details of the parametric study specimens: (a) column details, (b) 3D model, and (c) boundary conditions and applied load

4. Parametric Study Results

Table 2 and Figure 9 show the parametric study results obtained from the FE models for each compressive strength and slenderness ratios. From the results it can be noticed that rubber content has significant influence on both the ultimate load and the lateral deflection at ultimate load of column with

different slenderness ratios and control specimen strength; because of the effect of the rubber in reducing the concrete compressive and tensile strength and increasing the ductility of the rubbercrete column.

Table 2- Ultimate capacity and corresponding lateral deflection for all FE specimens.

No.	Specimen	Ultimate lateral deflection (U_L) (mm)	Ultimate capacity (P_u) (kN)
1	S-8-24-0	4.14	1309.92
2	S-8-24-5	8.07	1109.16
3	S-8-24-10	9.83	1058.32
4	S-8-24-20	9.57	926.77
5	S-15-24-0	14.01	1143.7
6	S-15-24-5	30.35	875.55
7	S-15-24-10	30.56	821.9
8	S-15-24-20	31.14	712.73
9	S-20-24-0	27.03	989.42
10	S-20-24-5	34.37	648.39
11	C-20-24-10	34.54	611.98
12	S-20-24-20	34.87	538.55
13	S-25-24-0	34.88	815.86
14	S-25-24-5	36.29	508.16
15	S-25-24-10	36.51	483.49
16	S-25-24-20	37.13	432.26
17	S-8-28-0	4.09	1472.88
18	S-8-28-5	9.06	1263.35
19	S-8-28-10	9.95	1169.84
20	S-8-28-20	9.67	1026.99
21	S-15-28-0	13.85	1280.44
22	S-15-28-5	30.11	972.99
23	S-15-28-10	30.33	913.11

Table 2- continued - Ultimate capacity and corresponding lateral deflection for all FE specimens.

No.	Specimen	Ultimate lateral deflection (U_L) (mm)	Ultimate capacity (P_u) (kN)
24	S-15-28-20	30.53	790.5
25	S-20-28-0	26.88	1105.37
26	S-20-28-5	33.44	708.59
27	S-20-28-10	33.56	668.99
28	S-20-28-20	34.56	589.37
29	S-25-28-0	33.81	896.75
30	S-25-28-5	35.45	554.23
31	S-25-28-10	35.78	525.98
32	S-25-28-20	36.83	467.74
33	S-8-60-0	7.58	2770.81
34	S-8-60-5	9.82	2292.79
35	S-8-60-10	9.85	2139.93
36	S-8-60-20	10.05	1813.99
37	S-15-60-0	24.34	2207.02
38	S-15-60-5	33.72	1602.15
39	S-15-60-10	33.63	1505.32
40	S-15-60-20	31.3	1310.98
41	S-20-60-0	30.22	1739.65
42	S-20-60-5	29.76	1096.18
43	S-20-60-10	29.91	1033.81
44	S-20-60-20	30	906.99
45	S-25-60-0	34.98	1309.32
46	S-25-60-5	33.53	898.23
47	S-25-60-10	33.24	844.95
48	S-25-60-20	33.01	734.02

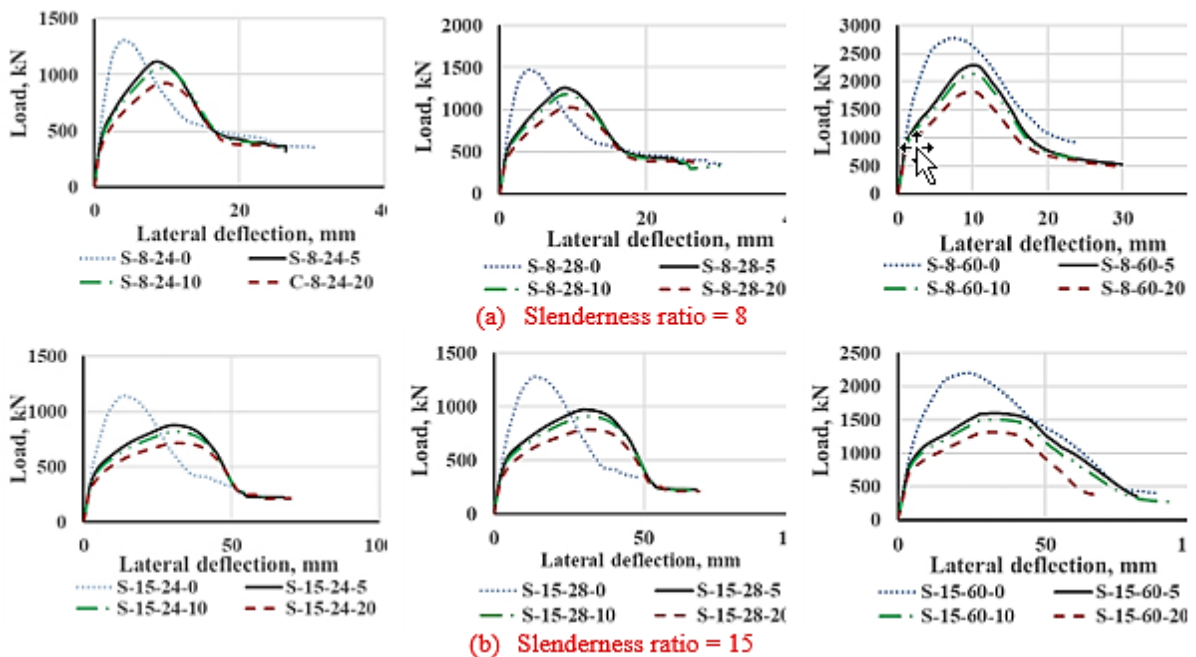


Figure 9- Load-lateral deflection relationship for FE specimens.

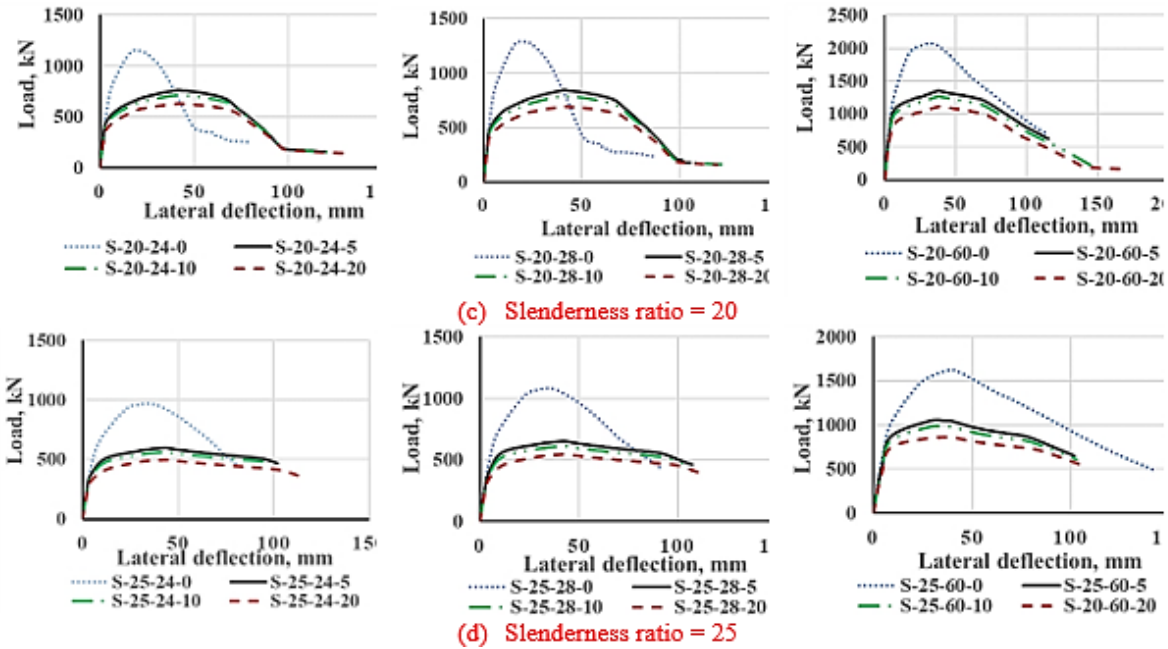


Figure 10- continued - Load-lateral deflection relationship for FE specimens.

4.1. Failure Mode

The failure mode observed in rubbercrete reinforced concrete columns primarily resulted from concrete crushing as shown in Figure 10, based on FE results

of example parametric study columns with varying concrete compressive strength and slenderness ratios.

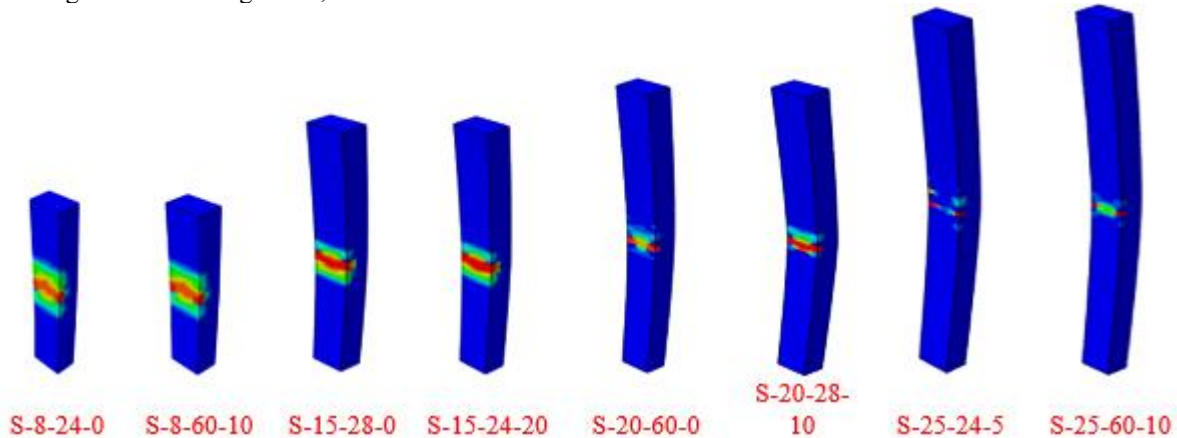


Figure 11- Failure modes of rubbercrete-reinforced concrete columns.

4.2. Effect of Slenderness Ratio

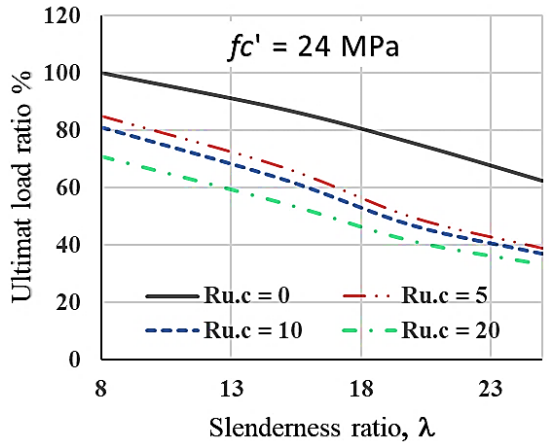
For the four different rubber content values, Figure 11 displays the relationships between the ultimate load ratios of the columns, derived from finite element analysis (FE), and their slenderness ratios for all compressive strength values. Furthermore, Figure 12 shows the lateral deflections at maximum load ratios plotted against slenderness ratios for all variations of rubber content and concrete strength. The study found that:

1. Decrease in Ultimate Capacity Ratio (Figure 11 & Table 2)

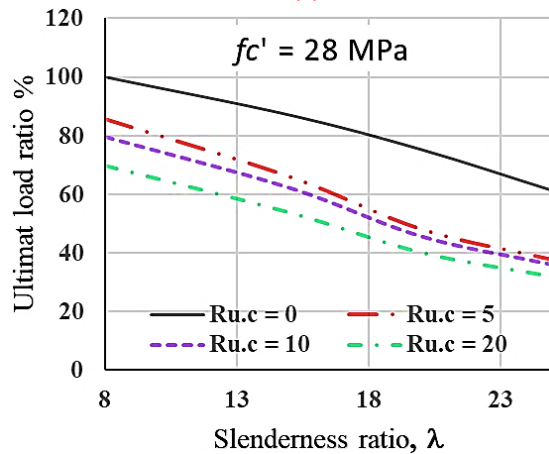
- As the slenderness ratio increased, the ultimate column capacity decreased. Specifically, for concrete strengths (f_c') of 24 MPa and 28 MPa, the capacities were reduced to 38% comparing columns S-8-24-0 and S-25-24-0 and 55%

comparing columns S-8-28-10 and S-25-28-10, respectively.

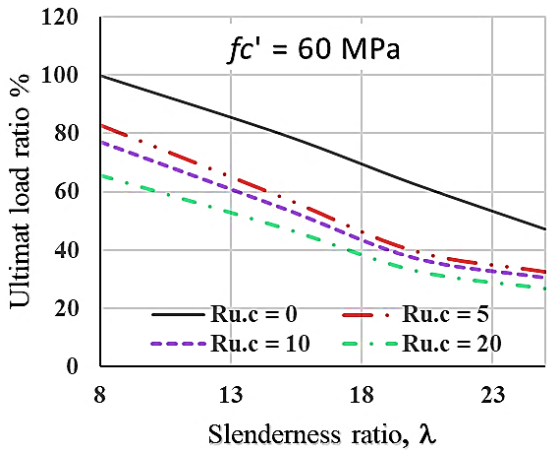
- In the case of $f_c' = 60$ MPa, the ultimate capacity reduced to 60% comparing columns S-8-60-20 and S-25-60-20.
- The relationship between slenderness ratio and the reduction of the ultimate load was gradually linear for normal concrete. However, for high-strength concrete, this linearity continued only up to a slenderness ratio $\lambda = 20$. After this point, the slope of the relationship was changed to be approximately constant, and changes in ultimate capacity ratios became negligible with varying rubber content ratio.



(a)



(b)



(c)

Figure 12- Influence of slenderness ratio on ultimate capacity ratio of concrete/rubbercrete columns at different compressive strengths: (a) $f_c' = 24$ MPa, (b) $f_c' = 28$ MPa, and (c) $f_c' = 60$ MPa. ($R_{u.c}$: rubber content)

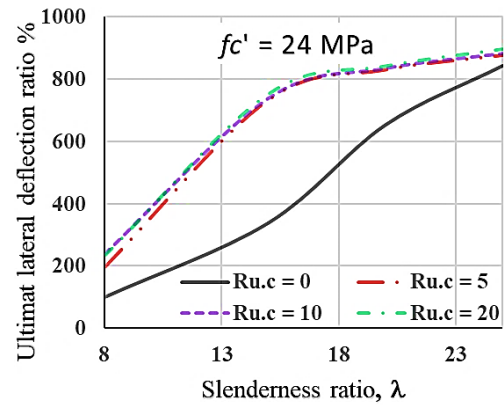
2. Increase in Lateral Deflection Ratio (Figure 12 & Table 2)

- As the slenderness ratio increased, the lateral deflection at the ultimate capacity also

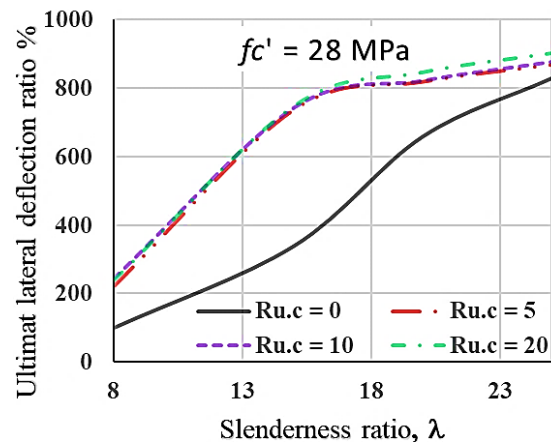
increased for all concrete strengths and rubber contents.

- The average increases of lateral deflection for $f_c' = 24$ MPa and 28 MPa were 8.4 times greater comparing columns S-8-24-0 and S-25-24-0 and 3.6 times greater comparing columns S-8-28-10 and S-25-28-10, respectively.
- For f_c' equals to 60 MPa, the deflection increased 3.3 times compared to columns S-8-60-20 and S-25-60-20.
- For normal rubbercrete, the lateral deflection at ultimate capacity ratio of column was increased gradually up to slenderness ratio (λ) = 16, after that the slop of increasing was changed to be nearest to constant and the value of increasing was near to that for normal concrete at slenderness ratio (λ) = 25. While for high strength rubbercrete the increasing of lateral ultimate deflection was approximately the same of high strength concrete after slenderness ratio (λ) = 20.

These studies illustrate the relationship between slenderness ratio and column performance, identifying that both the ultimate load capacity and lateral deflection are considerably influenced by variations in slenderness.



(a)



(b)

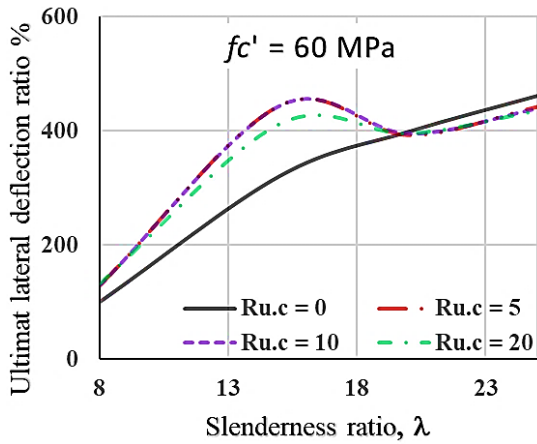


Figure 13- Influence of slenderness ratio on lateral deflection at ultimate capacity ratio of concrete/rubbercrete columns at different compressive strengths: (a) $f_c' = 24$ MPa, (b) $f_c' = 28$ MPa, and (c) $f_c' = 60$ MPa.

4.3. Effect of Rubber Content Ratio

Figure 13 and Figure 14 show the ultimate and lateral deflections of reinforced concrete/rubbercrete columns in relation to rubber content ratios for all slenderness ratios and concrete compressive strengths. The study showed that:

- Ultimate Capacity Ratio For all compressive strengths (24 MPa, 28 MPa, and 60 MPa) and slenderness ratios, the ultimate capacity decreases as the rubber content increases.
- The reduction in ultimate load capacity is significant, with a reduction of 29.2% for 24 MPa concrete comparing specimens S-8-24-0 and S-8-24-20 and 46.7% for 28 MPa comparing S-20-28-0 and S-20-28-20.
- For 60 MPa concrete, the reduction is more pronounced, with a value of 47.9% reduction in capacity when comparing columns S-20-60-0 and S-20-60-20.
- The energy dissipation capacity of rubbercrete is more than that of conventional concrete, especially in seismic or dynamic applications.

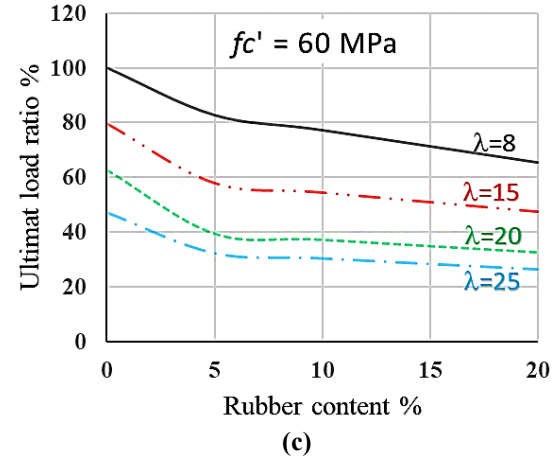
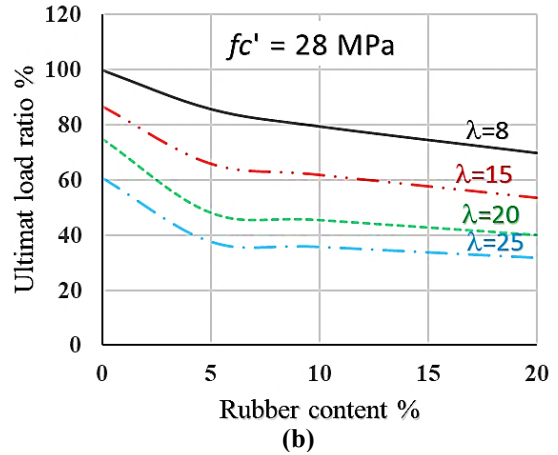
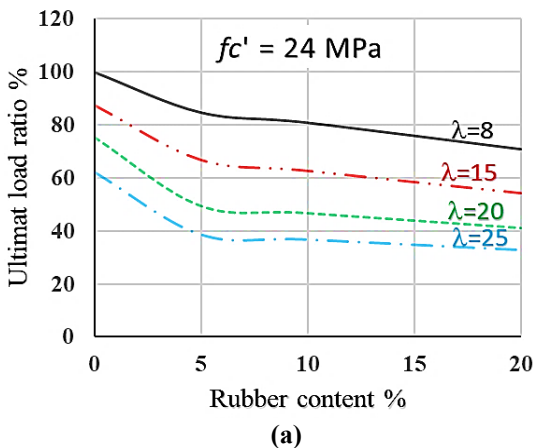
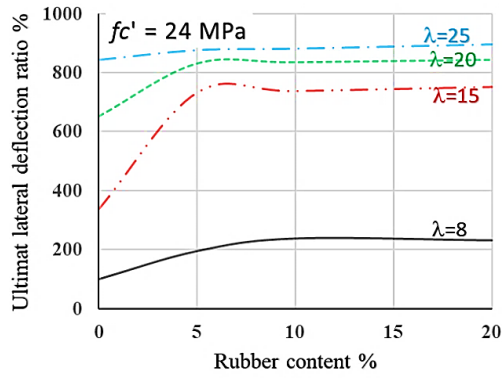


Figure 14- Influence of rubber content ratio on ultimate capacity ratio of concrete/rubbercrete columns at different compressive strengths: (a) $f_c' = 24$ MPa, (b) $f_c' = 28$ MPa, and (c) $f_c' = 60$ MPa.

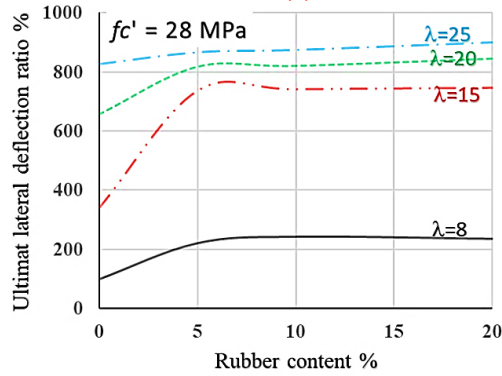
(d) Lateral Deflection Ratio (Figure 14 and Table 2)

- The lateral deflection at ultimate load generally increases with the rise in rubber content across all compressive strength categories and slenderness ratios. This is due to the lower compressive strength and reduced overall stiffness of the concrete containing rubber.
- For the cases of $f_c' = 24$ MPa and 28 MPa, the lateral deflection at ultimate load increased 2.3 times comparing specimens S-8-24-0 and S-8-24-20, increased 1.29 times comparing specimens S-20-28-0 and S-20-28-20, respectively.
- For $f_c' = 60$ MPa concrete, the lateral deflection had a minimal change comparing specimens S-20-60-0 and S-20-60-20.

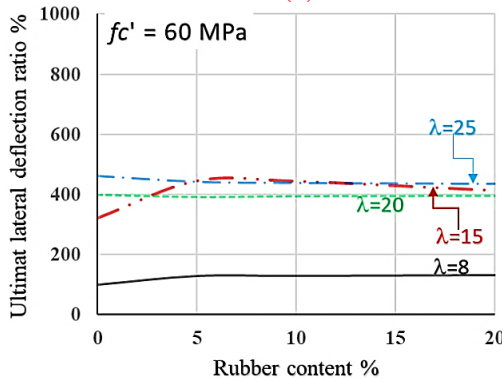
In both the ultimate capacity and lateral deflection, the most effective rubber content ratio was 5%. After this value, the changes in behavior become more dependent on the slenderness ratio. In practice rubbercrete is more suitable for applications where ductility is of prime importance, more than strength, such as the case of cyclic and seismic loads.



(a)



(b)



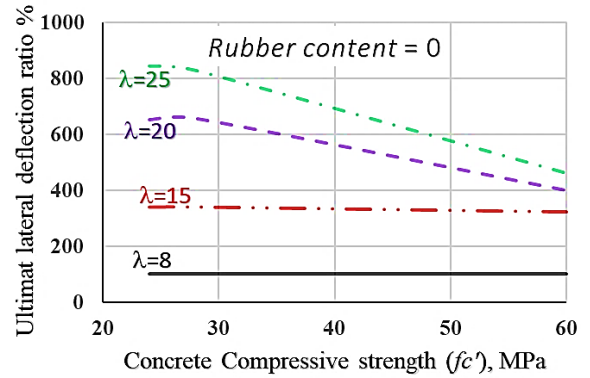
(c)

Figure 15- Influence of rubber content ratio on lateral deflection at ultimate capacity ratio of concrete/rubbercrete columns at different compressive strengths: (a) $f_c' = 24$ MPa, (b) $f_c' = 28$ MPa, and (c) $f_c' = 60$ MPa.

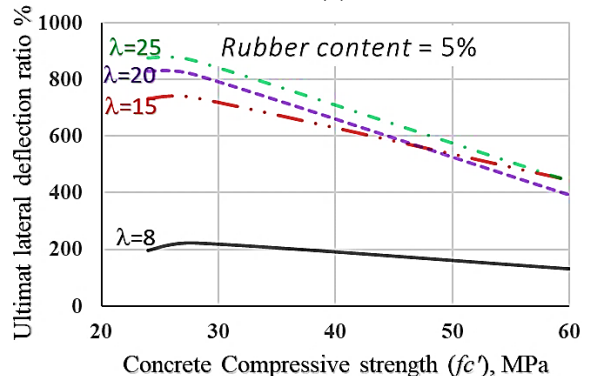
4.4. Effect of Concrete Compressive Strength

Figure 15 illustrates the relationships between lateral deflections at maximum loads, derived from finite element analysis (FE), and concrete compressive strengths for all rubber contents and slenderness ratios.

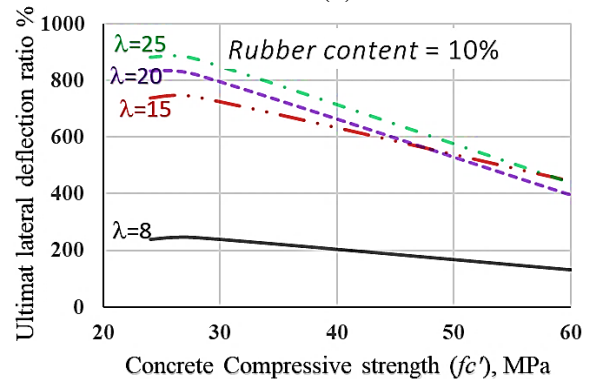
This result indicates that the increase in compressive strength improves the stiffness and stability of structures hence leads to decrease lateral deflection under load. Overall, these results have indicated that, in addition to compressive strength, an appropriate combination of rubber content is essential in influencing the performance characteristics of the rubbercrete column.



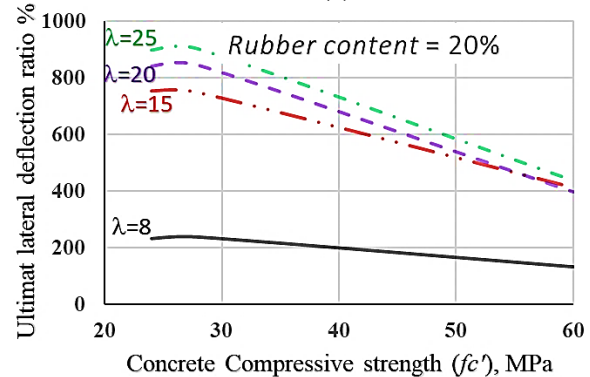
(a)



(b)



(c)



(d)

Figure 15- Influence of concrete/rubbercrete compressive strength on lateral deflection at ultimate capacity ratio of concrete/rubbercrete columns with different rubber content ratio: (a) rubber content = 0, (b) rubber content = 5%, (c) rubber content = 10%, and (d) rubber content = 20%.

5. Comparison Between Recorded Lateral Deflections and Equations of Codes

- Eurocode 2 (EC2) [31] provides the following equation for the total lateral deflection of long columns (δ):

$$\delta = e_0 + e_2 \tag{11}$$

Where,

$$e_0 = \frac{\text{first order bending}}{\text{first order axial force}} \tag{12}$$

e_2 : Second order eccentricity, and equals

$$e_2 = k_1 \frac{l_0^2}{10r} \tag{13}$$

Where,

$$k_1 = \frac{\lambda}{20} - 0.75 \tag{14}$$

λ : Slenderness ratio.

l_0 : Effective length of column and equals column length in our case.

$1/r$: Curvature.

r : Radius of gyration.

- The ECP203-2020 [30] code equation for estimating the lateral deflection value is as follows:

$$\delta = \frac{\lambda^2 * \text{side length}}{2000} \tag{15}$$

Table 3 presented the ultimate lateral deflection of normal concrete columns, of parametric study, obtained from FEM, Eurocode 2, and ECP203-2020, while Table 4 presents the same for the case of rubbercrete columns of parametric study. The lateral deflections for the specimens of the parametric study are examined as follows:

- For the columns of a slenderness ratio equal to 15, the lateral deflection increased from an average of 17.4 mm (as per Table 3) for three columns with no crumb (S-15-24-0, S-15-28-0 & S-15-60-0) to an average of 31.30 mm (as per Table 4) for the nine columns with crumb (S-15-24-5, S-15-24-10, S-15-24-20, S-15-28-5, S-15-28-10, S-15-28-20, S-15-60-5, S-15-60-10 & S-15-60-20). Eurocode 2 provides a maximum lateral deflection control of 20 mm, and the ECP203-2020 code provides a slavery of 22.5 mm of lateral deflection control. This means unsafe predictions from both codes for rubbercrete columns.
- For the case of a slenderness ratio of 20, the corresponding lateral deflections increased from 31.6 mm (Table 3) to 32.78 mm (Table 4) compared to the values of the codes which are 22.52 mm and 40 mm, respectively.
- For the case of slenderness ratio of 25, which is just outside the ECP203-2020 [30] code slenderness limit, the corresponding average lateral deflection increased from 34.56 mm (Table 3) to 35.31 mm (Table 4) compared to the values of the codes which are 25.04 mm and 62.5 mm, respectively.
- This means that the codes' equations for the lateral deflection need to be reconsidered for the case of slender columns made of concrete containing rubber. The amount of data in this research still needs to be enhanced by a very wide range of other research to enable the suggestion of code modifications.

Table 3- Comparison of ultimate lateral deflection of normal concrete column.

No.	Specimen	Ultimate lateral deflection; U_L (mm)		
		FEM	EC2	ECP207
1	S-8-24-0	5.27	-	6.4
2	S-8-28-0			
3	S-8-60-0			
4	S-15-24-0	17.4	20	22.5
5	S-15-28-0			
6	S-15-60-0			
7	S-20-24-0	31.6	22.52	40
8	S-20-28-0			
9	S-20-60-0			
10	S-25-24-0	34.56	25.04	62.5
11	S-25-28-0			
12	S-25-60-0			

Table 4- Comparison of ultimate lateral deflection of rubbercrete column.

No.	Specimen	Ultimate lateral deflection; U _L (mm)		
		FEM	EC2	ECP207
13	S-8-24-5	9.54	-	6.4
14	S-8-24-10			
15	S-8-24-20			
16	S-8-28-5			
17	S-8-28-10			
18	S-8-28-20			
19	S-8-60-5			
20	S-8-60-10			
21	S-8-60-20			
22	S-15-24-5	31.3	20	22.5
23	S-15-24-10			
24	S-15-24-20			
25	S-15-28-5			
26	S-15-28-10			
27	S-15-28-20			
28	S-15-60-5			
29	S-15-60-10			
30	S-15-60-20			
31	S-20-24-5	32.78	22.52	40
32	C-20-24-10			
33	S-20-24-20			
34	S-20-28-5			
35	S-20-28-10			
36	S-20-28-20			
37	S-20-60-5			
38	S-20-60-10			
39	S-20-60-20			
40	S-25-24-5	35.31	25.04	62.5
41	S-25-24-10			
42	S-25-24-20			
43	S-25-28-5			
44	S-25-28-10			
45	S-25-28-20			
46	S-25-60-5			
47	S-25-60-10			
48	S-25-60-20			

6. Conclusions

Based on the numerical analysis conducted in this study, the following major conclusions can be drawn:

1. Influence of Slenderness Ratio: Increasing the slenderness ratio decreased ultimate capacity but increased lateral deflection at ultimate capacity.
2. Influence of Rubber Content: Increasing rubber ratio in concrete mixture decreased ultimate column capacity and increased lateral deflection at ultimate load.
3. Influence of Concrete Strength: Increasing compressive strength led to lower lateral deflection ratios at ultimate loads in all cases.
4. Reconsideration of Code Equations: The equations provided by both Eurocode 2 and ECP203-2020 for estimating the lateral

deflection of long columns should be reconsidered when applied to crumb concrete.

NOTATIONS

- f'_c = Concrete peak strength.
- f_c = Concrete stress at any state of loading.
- ϵ = Concrete strain at any state of loading.
- ϵ_0 = Concrete strain at peak stress.
- E_c = Elastic modulus of concrete.
- β, k_1 & k_2 = Factors.
- f_{ct} = Tensile strength of concrete.
- w_c = Crack opening.
- G_F = Total external energy input per unit area which creates crack of mode I.
- $\alpha_0 = 1.44$ for crushed or angular aggregates.
- d_a = Aggregate diameter.
- w/c = Water cement ratio.

E_s = Elastic modulus for steel.

f_s = Steel stress.

ε_s = Steel strain.

f_{sy} = Yield stress of steel.

λ = Slenderness ratio.

e_2 = Second order eccentricity.

l_0 = Effective length of column.

$1/r$ = The curvature.

r = The radius of gyration.

7. References

- [1] G. Li, M. A. Stubblefield, G. Garrick, J. Eggers, C. Abadie, and B. Huang, "Development of Waste Tire Modified Concrete" *Cement and Concrete Research*, 2004, V. 34, No. 12, pp. 2283-2289, <https://doi.org/10.1016/j.cemconres.2004.04.013>.
- [2] N. N. Eldin, and A. B. Senouci, "Rubber-Tire Particles as Concrete Aggregate" *Journal of Materials in Civil Engineering*, 1993, V. 5, No. 4, pp. 478-496, [https://doi.org/10.1061/\(ASCE\)0899-1561\(1993\)5:4\(478\)](https://doi.org/10.1061/(ASCE)0899-1561(1993)5:4(478)).
- [3] N. N. Eldin, and A. B. Senouci, "Measurement and Prediction of the Strength of Rubberized Concrete" *Cement and Concrete Composites*, 1994, V. 16, No. 4, pp. 287-298, [https://doi.org/10.1016/0958-9465\(94\)90041-8](https://doi.org/10.1016/0958-9465(94)90041-8).
- [4] Z. K. Khatib, and F. M. Bayomy, "Rubberised Portland Cement Concrete" *Journal of Materials in Civil Engineering*, 1999, V. 11, No. 3, pp. 206-213, [https://doi.org/10.1061/\(ASCE\)0899-1561\(1999\)11:3\(206\)](https://doi.org/10.1061/(ASCE)0899-1561(1999)11:3(206)).
- [5] M. M. T. Reda, A. S. El-Dieb, M. A. El-Wahab, and M. E. Abdel-Hameed, "Mechanical Fracture and Microstructural Investigations of Rubber Concrete" *Journal of Materials in Civil Engineering*, 2008, V. 20, No. 10, pp. 640-649, [https://doi.org/10.1016/0958-9465\(94\)90041-8](https://doi.org/10.1016/0958-9465(94)90041-8).
- [6] I. B. Topçu, "The Properties of Rubberized Concretes" *Cement and Concrete Research*, 1995, V. 25, No. 2, pp. 304-310, [https://doi.org/10.1016/0008-8846\(95\)00014-3](https://doi.org/10.1016/0008-8846(95)00014-3).
- [7] B. Huang, G. Li, S. Pang, and J. Eggers, "Investigation into Waste Tire Rubber-Filled Concrete" *Journal of Materials in Civil Engineering*, 2004, V. 16, No. 3, pp. 187-194, DOI: [10.1061/\(ASCE\)0899-1561\(2004\)16:3\(187\)](https://doi.org/10.1061/(ASCE)0899-1561(2004)16:3(187)).
- [8] G. Li, G. Garrick, J. Eggers, C. Abadie, M. A. Stubblefield, and S. S. Pang, "Waste Tire Fiber Modified Concrete" *Composites Part B: Engineering*, 2004, V. 35, No. 4, pp. 305-312, <https://doi.org/10.1016/j.compositesb.2004.01.002>.
- [9] I. B. Topçu, and M. Sarıdemir, "Prediction of Rubberized Concrete Properties using Artificial Neural Networks and Fuzzy Logic" *Construction and Building Materials*, 2008, V. 22, No. 4, pp. 532-540, DOI: [10.1016/j.conbuildmat.2006.11.007](https://doi.org/10.1016/j.conbuildmat.2006.11.007).
- [10] A. R. Khaloo, M. Dehestani, and P. Rahmatabadi, "Mechanical Properties of Concrete Containing a High Volume of Tire-Rubber Particles" *Waste Management*, 2008, V. 28, No. 12, pp. 2472-2482, <https://doi.org/10.1016/j.wasman.2008.01.015>.
- [11] R. Siddique, and T. R. Naik, "Properties of Concrete Containing Scrap-Tire Rubber – an Overview" *Waste Management*, 2004, V. 24, No. 6, pp. 563-569, DOI: [10.1016/j.wasman.2004.01.006](https://doi.org/10.1016/j.wasman.2004.01.006).
- [12] F. Hernández-Olivares, G. Barluenga, M. Bollati, and B. Witoszek, "Static and Dynamic Behaviour of Recycled Tyre Rubber-Filled Concrete" *Cement and Concrete Research*, 2002, V. 32, No. 10, pp. 1587-1596, [https://doi.org/10.1016/S0008-8846\(02\)00833-5](https://doi.org/10.1016/S0008-8846(02)00833-5).
- [13] A. Gregori, C. Castoro, M. Mercuri, and M. Angiolilli, "Numerical Modelling of the Mechanical Behaviour of Rubbercrete" *Computers & Structures*, 2021, 242, 106393. <https://doi.org/10.1016/j.compstruc.2020.106393>.
- [14] A. Mohajerani, et al., "Recycling Waste Rubber Tyres in Construction Materials and Associated Environmental Considerations: A Review" *Resources, Conservation and Recycling*, 2020, 155, 104679, <https://doi.org/10.1016/j.resconrec.2020.104679>.
- [15] J. Mei, et al., "Promoting Sustainable Materials using Recycled Rubber in Concrete: A Review" *Journal of Cleaner Production*, 2022, 373, 133927, <https://doi.org/10.1016/j.jclepro.2022.133927>.
- [16] A. Hamdi, G. Abdelaziz, and K. Z. Farhan, "Scope of Reusing Waste Shredded Tires in Concrete and Cementitious Composite

- Materials: A Review". *Journal of Building Engineering*, 2021, 35, 102014, <https://doi.org/10.1016/j.jobe.2020.102014>.
- [17] S. Surehali, A. Singh, and K. P. Biligiri, "A State-of-the-Art Review on Recycling Rubber in Concrete: Sustainability Aspects, Specialty Mixtures, and Treatment Methods" *Developments in the Built Environment*, 2023, 14, 100171, <https://doi.org/10.1016/j.dibe.2023.100171>.
- [18] N. Fauzan, K. Albarqi, A. P. Melinda, and Z. Al Jauhari, "The Effect of Waste Tyre Rubber on Mechanical Properties of Normal Concrete and Fly Ash Concrete" *International Journal of GEOMATE*, 2021, V. 20, No. 77, pp. 55-61, DOI: <https://doi.org/10.21660/2023.108.3838>.
- [19] S. Muhammad, et al., "Fresh and Hardened Properties of Waste Rubber Tires Based Concrete: a State Art of Review". *SN Applied Sciences*, 2023, 5, 119, <https://doi.org/10.1007/s42452-023-05336-5>.
- [20] M. Shahjalal, et al., "Fiber-Reinforced Recycled Aggregate Concrete with Crumb Rubber: A State-of-the-Art Review". *Construction and Building Materials*, 2023, 404, 133233, <https://doi.org/10.1016/j.conbuildmat.2023.133233>.
- [21] A. Pal, K. S. Ahmed, F. Z. Hossain, and M. S. Alam, "Machine Learning Models for Predicting Compressive Strength of Fiber-Reinforced Concrete Containing Waste Rubber and Recycled Aggregate". *Journal of Cleaner Production*, 2023, 423, 138673, <https://doi.org/10.1016/j.jclepro.2023.138673>.
- [22] R. Shao, et al., "Mechanical Behavior and Environmental Benefit of Eco-Friendly Steel Fibre-Reinforced Dry UHPC Incorporating High-Volume Fly Ash and Crumb Rubber" *Journal of Building Engineering*, 2023, 65, 105747, <https://doi.org/10.1016/j.jobe.2022.105747>.
- [23] O. Youssf, A. Swilam, and A. M. Tahwia, "Performance of Crumb Rubber Concrete Made with High Contents of Heat Pre-Treated Rubber and Magnetized Water" *Journal of Materials Research and Technology*, 2023, 23, pp. 2160-2176, <https://doi.org/10.1016/j.jmrt.2023.01.146>.
- [24] O. Youssf, M. A. ElGawady, and J. E. Mills, "Experimental Investigation of Crumb Rubber Concrete Columns under Seismic Loading" *Structures*, 2015, 3, pp. 13-27. <https://doi.org/10.1016/j.istruc.2015.02.005>.
- [25] K. S. Son, I. Hajirasouliha, and K. Pilakoutas, "Strength and Deformability of Waste Tyre Rubber-Filled Reinforced Concrete Columns" *Construction and Building Materials*, 2011, V. 25, No. 1, pp. 218-226, <https://doi.org/10.1016/j.conbuildmat.2010.06.035>.
- [26] Dassault Systems, "ABAQUS, Analysis User's Manual" 2012
DOI: [10.4236/jmp.2020.112020](https://doi.org/10.4236/jmp.2020.112020).
- [27] T. Wee, M. Chin, and M. Mansur, "Stress-Strain Relationship of High-Strength Concrete in Compression" *Journal of Materials in Civil Engineering*, 1996, V. 8, No. 2, pp. 70-76, [https://doi.org/10.1061/\(ASCE\)0899-1561\(1996\)8:2\(70\)](https://doi.org/10.1061/(ASCE)0899-1561(1996)8:2(70)).
- [28] F. Aslani, G. Ma, D. L. Y. Wan, and V. X. T. Le, "Experimental Investigation into Rubber Granules and their Effects on the Fresh and Hardened Properties of Self-Compacting Concrete" *Journal of Cleaner Production*, 2018, 172, pp. 1835-1847, <https://doi.org/10.1016/j.jclepro.2017.12.003>.
- [29] C. A. Coronado, and M. M. Lopez, "Sensitivity Analysis of Reinforced Concrete Beams Strengthened with FRP Laminates". *Cement and Concrete Composites*, 2006, V. 28, No. 1, pp. 102-114.
[doi:10.1016/j.cemconcomp.2005.07.005](https://doi.org/10.1016/j.cemconcomp.2005.07.005).
- [30] Committee for Egyptian Concrete Code, "Egyptian Code for Design and Construction of Reinforced Concrete Structures (ECP203-2020)" Housing and Building National Research Center, 2020, Giza, Egypt.
- [31] Eurocode 2 Committee, "Eurocode 2-Part 1: Design of Concrete Structures (ENV 1992-1-1:1992)" European Standards, Brussels, Belgium, 2004, 195 p.